

# Investigation of Water Evaporation Process at Air/Water Interface using Hofmeister Ions

Bhawna Rana<sup>†</sup>, David J. Fairhurst<sup>‡</sup>, and Kailash C. Jena<sup>\*,†,§</sup>

<sup>†</sup>Department of Physics and <sup>§</sup>Department of Biomedical Engineering, Indian Institute of Technology Ropar, Rupnagar, Punjab-140001, India

<sup>‡</sup>Department of Physics and Mathematics, School of Science and Technology, Nottingham Trent University, Nottingham, Clifton Campus, NG11 8NS, United Kingdom

**KEYWORDS** (*Water, Evaporation, Interface, sum frequency generation, Hofmeister Ions, H-bonding, Free OH*).

---

**ABSTRACT:** Evaporation is an interfacial phenomenon in which a water molecule breaks the intermolecular hydrogen (H-) bonds and enters the vapor phase. However, a detailed demonstration of the role of interfacial water structure in the evaporation process is still lacking. Here, we purposefully perturb the H-bonding environment at the air/water interface by introducing kosmotropic ( $\text{HPO}_4^{-2}$ ,  $\text{SO}_4^{-2}$ , and  $\text{CO}_3^{-2}$ ) and chaotropic ions ( $\text{NO}_3^-$  and  $\text{I}^-$ ) to influence the evaporation process. Using time-resolved interferometry on aqueous salt-droplets, we found that kosmotropes reduce evaporation, whereas chaotropes accelerate the evaporation process, following the Hofmeister series  $\text{HPO}_4^{-2} < \text{SO}_4^{-2} < \text{CO}_3^{-2} < \text{Cl}^- < \text{NO}_3^- < \text{I}^-$ . In order to extract deeper molecular level insights about the observed Hofmeister trend in the evaporation rates, we investigated the air/water interface in the presence of ions using surface-specific sum frequency generation (SFG) vibrational spectroscopy. The SFG vibrational spectra reveal the significant impact of ions on the strength of the H-bonding environment and on the orientation of free OH oscillators at the air/water interface, where both affects follow the Hofmeister series. It is established that in the presence of kosmotropes the slow evaporating water molecules experience a strong H-bonding environment with the free OH oscillators tilted away from the surface normal. In contrast, the fast evaporating water molecules in the presence of chaotropes experience a weak H-bonding environment with free OH oscillators tilted towards the surface normal at the air/aqueous interface. Our experimental outcomes showcase the complex bonding environment of interfacial water molecules and their decisive role in evaporation at the air/water interface.

---

## INTRODUCTION

Understanding and controlling water evaporation is of great importance in diverse fields of science and technology, including surface patterning, optical mapping of DNA molecules, biological activity on Mars, separating crude oil from water, water harvesting, and disease diagnosis in pharmaceutical industries.<sup>1-6</sup> In the domain of environmental sciences, the rate of evaporation of water molecules from the surface of aqueous aerosols decides the formation or growth of cloud droplets, which plays an indispensable role in maintaining the earth's water cycle and global temperature.<sup>7-9</sup> Thus, understanding water evaporation is of general interest. Despite the prevailing importance of evaporation in our daily lives, the molecular-level understanding of this phenomenon is still speculative. The water molecule breaks its hydrogen bonds (H-bonds) with neighboring molecules and leaves the interface to enter the air during the evaporation process. It is worth emphasizing that the interfacial molecular structure of water is quite different from the bulk, displaying a constellation of mono-, di-, tri-, and tetra- coordinated water species, with dangling/free OH, weakly H-bonded, and strongly H-bonded water molecules.<sup>10</sup> <sup>11</sup> Therefore, the H-bonding environment of the interfacial water molecules carries the potential to play a vital role in the evaporation process.

Previous studies of the evaporation of water droplets have shown the influence of co-solvents, gravity, and magnetic fields on evaporation dynamics.<sup>12-15</sup> Recently, Li *et al.*<sup>13</sup> and Edwards *et al.*<sup>15</sup> observed that gravity reverses the convective flows within evaporating binary micro-droplets. Furthermore, it is also demonstrated that the presence of a magnetic field affects the thermo-solutal advection and enhances the evaporation rates of paramagnetic aqueous droplets.<sup>14</sup> Evidently, these studies present an understanding of the evaporation phenomenon through macroscopic diffusion, thermal convection, and solutal advection. Molecular dynamics (MD) simulation studies have attempted to develop a molecular-level understanding of the process.<sup>16-19</sup> For example, Varillay *et al.* have shown that evaporation can be considered as a ballistic escape from the liquid surface where molecules in the higher energy tail of the Boltzmann's distribution are more susceptible to breaking free.<sup>16</sup> According to Mason, the water species having H-bond coordination number one and two possess sufficient energy to escape from the liquid surface.<sup>17</sup> Recently, Nagata *et al.* reported that exactly 44fs after an H-bond formation, two oscillating water molecules are at the closest approach, and provide a sufficiently strong energetic kick to a third molecule to eject it from the surface.<sup>18</sup> In addition, Musolino *et al.* proposed that the orientation of surface water molecules can also influence the evaporation kinetics.<sup>19</sup> The prevailing literature

highlights the importance of how the detailed H-bonding environment and orientation of water molecules is required for a complete mechanistic depiction of the evaporation process. The contribution of free OH (dangling) groups that constitute more than 20% of the population at the topmost water layer of the air/water interface<sup>20</sup> towards the evaporation process is not explored yet. This prompted us to offer a detailed experimental demonstration with quantitative analysis to reveal the role of interfacial water molecules and their bonding environment in the evaporation process.

In the present study, we build a comprehensive understanding of the evaporation phenomenon by probing the conformation and H-bonding environment of water molecules at the air/water interface. The H-bonded network can be easily perturbed in the presence of guest moieties.<sup>10-11, 21-24</sup> We have used this fact and purposefully employed a series of Hofmeister sodium salts; the selected anions are as follows:



Franz Hofmeister reported this series in 1888 in which ions are ordered according to their capacity to precipitate proteins from their aqueous solution.<sup>25</sup> The ions to the left of chloride ion are known as kosmotropes (structure-makers) while those to the right as chaotropes (structure-breakers).<sup>25-31</sup> The ions have a significant structuring effect on the bonding environment of water molecules at the air/water interface. Therefore, we have selectively utilized the influence of Hofmeister ions to tune the interfacial structure of water molecules to extract new molecular-level insights about the evaporation process.

Here, we first studied the impact of Hofmeister ions on evaporation dynamics of sessile water droplets using an in-house time-resolved interferometry setup. It is observed that the kosmotropes impede evaporation, whereas chaotropes accelerate the evaporation rate compared to the pristine air/water interface. The observed ion-specific variation in the evaporation rates is ascribed to the variation in interfacial water structure as investigated by Sum frequency generation (SFG) vibrational spectroscopy. We have performed orientation angle calculation for free OH oscillator at air/aqueous interface in the presence of ions to see their influence on evaporation. It is found that the kosmotropes promote strongly H-bonded water species at the interface with free OH oscillators tilted away from the surface normal reflects the signature of slowing down the evaporation process. In contrast, the presence of chaotropes brings weakly bonded water species with free OH oscillator tilted more towards the surface normal, accelerating the evaporation.

## EXPERIMENTAL SECTION

### Materials

In the present work, we have performed experiments with six inorganic sodium salts ( $\text{Na}_2\text{HPO}_4$ ,  $\text{Na}_2\text{SO}_4$ ,  $\text{Na}_2\text{CO}_3$ ,  $\text{NaCl}$ ,  $\text{NaNO}_3$ , and  $\text{NaI}$ ), purchased from Sigma Aldrich and used without any further purification.

### Time-Resolved Interferometry

Figure 1a presents the experimental setup of time-resolved interferometry used to estimate the evaporation rate of sessile droplets. In this setup, a low-power He-Ne laser beam ( $\lambda = 543 \text{ nm}$ ) is directed onto the surface of a droplet sitting on a glass prism of refractive index 1.5.

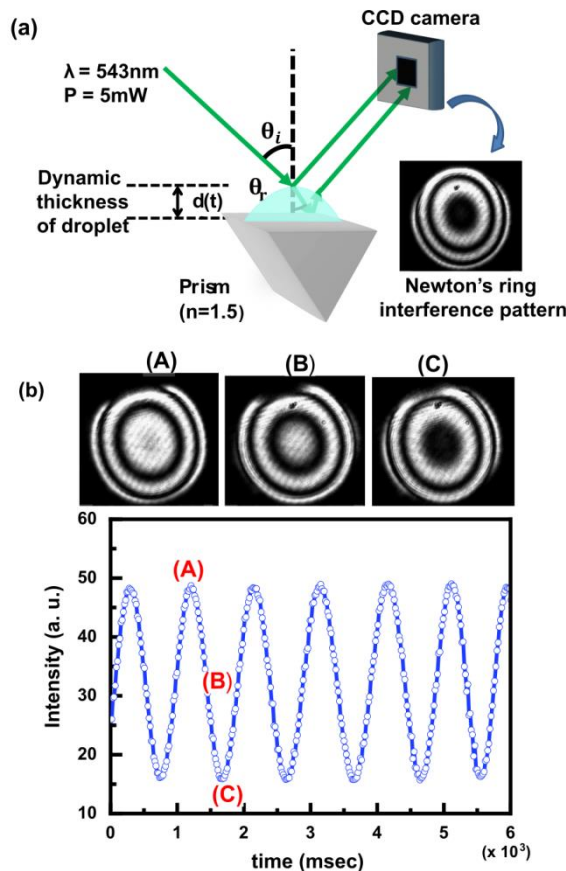


Figure 1. (a) Schematic of time-resolved interferometry for the evaporation rate studies of sessile aqueous droplets. (b) The snapshots with the intensity of the central fringe of the dynamic Newton's ring pattern with the time sequence of one fringe collapse (marked as A, B, and C, respectively).

The Fresnel reflections generated from the top and bottom surfaces form a Newton's ring interference pattern. The intensity of the interference pattern was recorded using a CCD camera for subsequent analysis. As the droplet is continuously evaporating, the droplet's moving surface, of height ( $d$ ) leads to a dynamic optical path and consequently a varying phase difference between the interfering beams, which is given by:<sup>32</sup>

$$\Delta\phi(t) = \frac{2\pi}{\lambda} \left( \frac{2n_1 d(t)}{\cos\theta_r} \right) \quad (2)$$

Here,  $n_1$  is the refractive index of the liquid medium and  $\theta_r$  ( $\sim 8^\circ$ ) the angle of refraction. The intensity of the central fringe pattern as a function of time is given by:<sup>32</sup>

$$I(t) \propto \cos^2(\Delta\phi(t)) \quad (3)$$

The variation in the intensity of the central fringe of the interference pattern is shown in figure 1b, with snapshots at various stages of one fringe cycle designated by A, B, and C, re-

spectively. The variable intensity profile is then utilized to calculate the change in droplet height  $\Delta d(t)$  as follows. The variation in the central fringe intensity from one maximum (or minimum) to the next, results in a phase change of  $\Delta\phi = 2\pi$ , thus moving over  $(k+1)$  maxima gives a change in droplet thickness as given by:

$$\Delta d(t) = k \left( \frac{\lambda \cos\theta_r}{2n_1} \right) \quad (4)$$

Here,  $k$  is an integer having values 0, 1, 2, 3 etc. Plotting  $\Delta d(t)$  with time gives a straight line plot, the slope of which measures the evaporation rate. In the present experiments, we have performed evaporation rate studies with 20  $\mu\text{l}$  aqueous sessile droplets of pristine water and 1M sodium salt solutions. All the solutions are prepared in deionized water (Merck, Millipore direct-Q3, electrical resistivity of 18  $\text{M}\Omega\cdot\text{cm}$ ).

### Surface Tension Studies

We have performed surface tension measurements of the aqueous samples by employing the Wilhelmy plate method using Biolin Scientific KSV NIMA Langmuir-Blodgett apparatus. The system consists of a platinum (Pt) plate which is dipped into aqueous samples in a Teflon sample cell ( $\sim 5$  cm diameter and 7 ml capacity). The Pt plate is rinsed thoroughly with ethanol and deionized water before use. All samples are prepared in deionized water and the measurements are conducted in the lab temperature of  $21.5 \pm 0.5^\circ\text{C}$ .

### Sum Frequency Generation Vibrational Spectroscopy

In the present study, we used an SFG Spectrometer (EKSPLA, Lithuania, SFG061) consisting of a mode-locked Nd:YAG picosecond diode pumped solid state (DPSS) laser system (PL2231-50), which provides a 30ps infrared (IR) beam at 1064 nm with output energy 40mJ at a repetition rate of 50 Hz. This fundamental beam is then used in the second harmonic generation unit (SFGH500-2H) to generate the visible beam at 532 nm. The fundamental (1064 nm) and the second harmonic (532 nm) beams then fed to the optical parametric generation unit (PG501-DFG2) that generates the tunable IR from 2300 nm to 16000 nm in the output. This visible 532 nm beam (diameter  $\sim 200$   $\mu\text{m}$  with 500  $\mu\text{J}$  energy/pulse) and tunable IR beam (diameter  $\sim 150$   $\mu\text{m}$  with 235  $\mu\text{J}$  energy/pulse at 3000 nm) were incident on the sample surface at angles around  $63^\circ$  and  $56^\circ$ , respectively with respect to the surface normal. The resultant sum frequency signal reflected at an angle of  $61^\circ$  is then directed through the detection optics. The intensity of the SFG signal is given as: <sup>28-29, 33-40</sup>

$$I \propto |\chi^{(2),\text{eff}}|^2 I_1 I_2 \quad (5)$$

Here,  $I_1$  and  $I_2$  are the intensities of visible and IR beams.  $\chi^{(2),\text{eff}}$  is a second-order nonlinear susceptibility tensor and can be expressed as:

$$\chi^{(2),\text{eff}} = \chi_{\text{NR}}^{(2)} + \sum_v \frac{A_v}{(\omega_v - \omega_2 - i\Gamma_v)} \quad (6)$$

Here,  $\chi_{\text{NR}}^{(2)}$  is the non-resonant component of the susceptibility, and the second term is the resonant part represented by a Lo-

rentzian function. Resonance occurs when  $\omega_2$  (IR frequency) matches with the vibrational characteristic frequency ( $\omega_v$ ) of the molecules present at the interface. Here,  $A_v$  and  $\Gamma_v$  are the amplitude and the half-width at half maxima (HWHM) of the Lorentzian line shape respectively. All the SFG spectra are collected in different polarization schemes (ssp and ppp) in the OH stretching region from 2800 to 3800  $\text{cm}^{-1}$  at a step size of 2  $\text{cm}^{-1}$  and acquisition per step of 200 and are fitted with Lorentzian line shape using equations (5-6). All the aqueous samples for SFG measurements are prepared in deionized water. We used a Teflon sample cell (diameter  $\sim 5$ cm) to hold the aqueous sample for SFG measurements. The sample cell is cleaned every time before the experiment using a piranha solution (3:1 v/v of concentrated sulphuric acid to 30% hydrogen peroxide solution) and then rinsed thoroughly with deionized water. All the experiments are conducted in the lab temperature of  $21.5 \pm 0.5^\circ\text{C}$ .

### RESULTS AND DISCUSSION

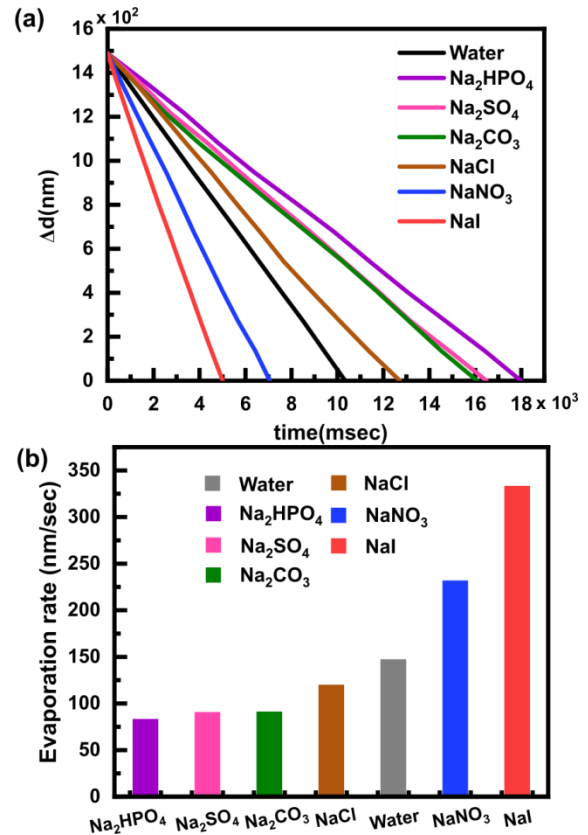


Figure 2. (a) Change in droplet central thickness ( $\Delta d$ ) vs. time for sessile aqueous droplets of pristine water and 1M sodium salt solutions. The slopes of these experimental plots provide evaporation rates at the air/aqueous interface (panel (b)).

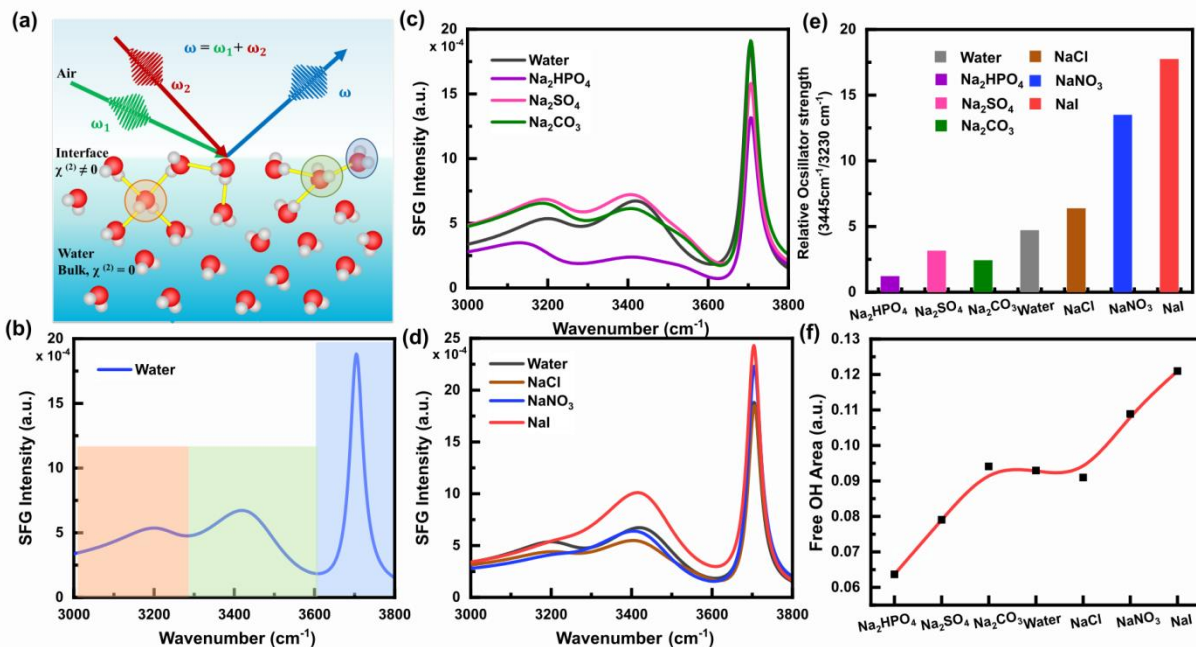


Figure 3. (a) Sketch of SFG vibrational spectroscopic experiments on air/aqueous interface. (b) SFG spectrum collected from pristine air/water interface in ssp polarization scheme; water species contributing into the shaded region of the spectrum are presented in panel (a). Polarization scheme ssp designates s-SFG, s-visible, and p-polarization of IR beams. Panel (c) and (d) SFG spectra at air/aqueous interface in the presence of 1M Hofmeister series sodium salts. The curves are Lorentzian fitted profiles; the fitting parameters are provided in table S2. Panel (e) and (f) represent the variation in relative oscillator strength (amplitude ratio of SFG peaks at 3445  $\text{cm}^{-1}$  and 3230  $\text{cm}^{-1}$ ) and the integrated area under the free OH peak (3660  $\text{cm}^{-1}$  to 3750  $\text{cm}^{-1}$ ) as a function of ions at the air/aqueous interface.

Figure 2a shows plots of change in central thickness  $\Delta d(t)$  vs.  $t$  for aqueous droplets of pristine water and for different sodium salt solutions with initial concentration of 1M. The slopes of these plots are utilized to quantify the evaporation rate values. The ion-specific evaporation rates of sessile droplets (figure 2b) follow the Hofmeister series as follows:

$$\text{HPO}_4^{-2} < \text{SO}_4^{-2} < \text{CO}_3^{-2} < \text{Cl}^- < \text{NO}_3^- < \text{I}^- \quad (7)$$

with a minimum evaporation rate for  $\text{Na}_2\text{HPO}_4$  (83 nm/sec) and a maximum evaporation rate for NaI (333 nm/sec). Evidently, the presence of kosmotropes ( $\text{HPO}_4^{-2}$ ,  $\text{SO}_4^{-2}$ , and  $\text{CO}_3^{-2}$ ) impedes the evaporation, whereas the presence of chaotropes ( $\text{NO}_3^-$  and  $\text{I}^-$ ) accelerate the evaporation rate at the air/aqueous interface compared to the pristine water droplet (147 nm/sec). We have also carried out salt concentration-dependent evaporation rate studies on aqueous sessile droplets. The results are shown in section S2-I of supporting information. The evaporation rate decreases with the increase in the salt concentration, and the overall trend for various salts follows the similar Hofmeister series. The findings from the time-resolved interferometry experiment confirm the significant impact of ions on the evaporation process.

One explanation for the observed variation in the evaporation rate of aqueous sessile droplets could be the impact of ions on the surface tension of water. To investigate this hypothesis, we carried out surface tension measurements of 1M sodium salt solutions (figure S2). We observed that the presence of salts increased the surface tension following a Hofmeister trend. This implies that the net effective pull on the surface water molecules from the molecules of the bulk is enhanced for sodium salt solutions compared to purewater. Accordingly, water molecules require more energy to overcome the high surface tension and evaporate, and by Gibb's energy theorem is a less thermodynamically favorable event. Recalling figure 2, the high surface tension justifies slower evaporation rates in the presence of kosmotropes, but fails to explain the higher evaporation rates in the presence of chaotropes as compared to the neat water interface. This suggests that we cannot solely rely on the macroscopic surface tension to explain the evaporation dynamics. We require a detailed molecular-level probing of the H-bonding environment of the water molecules at the air/aqueous interface to develop a mechanistic understanding of the evaporation process.

To gain such a detailed molecular-level understanding of the observed Hofmeister trend in the evaporation rate, we have employed SFG vibrational spectroscopy to probe the influence of ions on interfacial water structure. The schematic layout of the SFG experi-

ments is presented in figure 3a. SFG vibrational spectroscopy is an ideal spectroscopic tool to selectively probe the conformation and the structure of moieties in the interfacial region and is based on second-order nonlinear optical process.<sup>28-29, 33-40</sup> We consider the SFG spectrum at the pristine air/water interface as the reference spectrum to observe the comparative impact of various salts (Figure 3b). The spectra (Figure 3b-d) contain

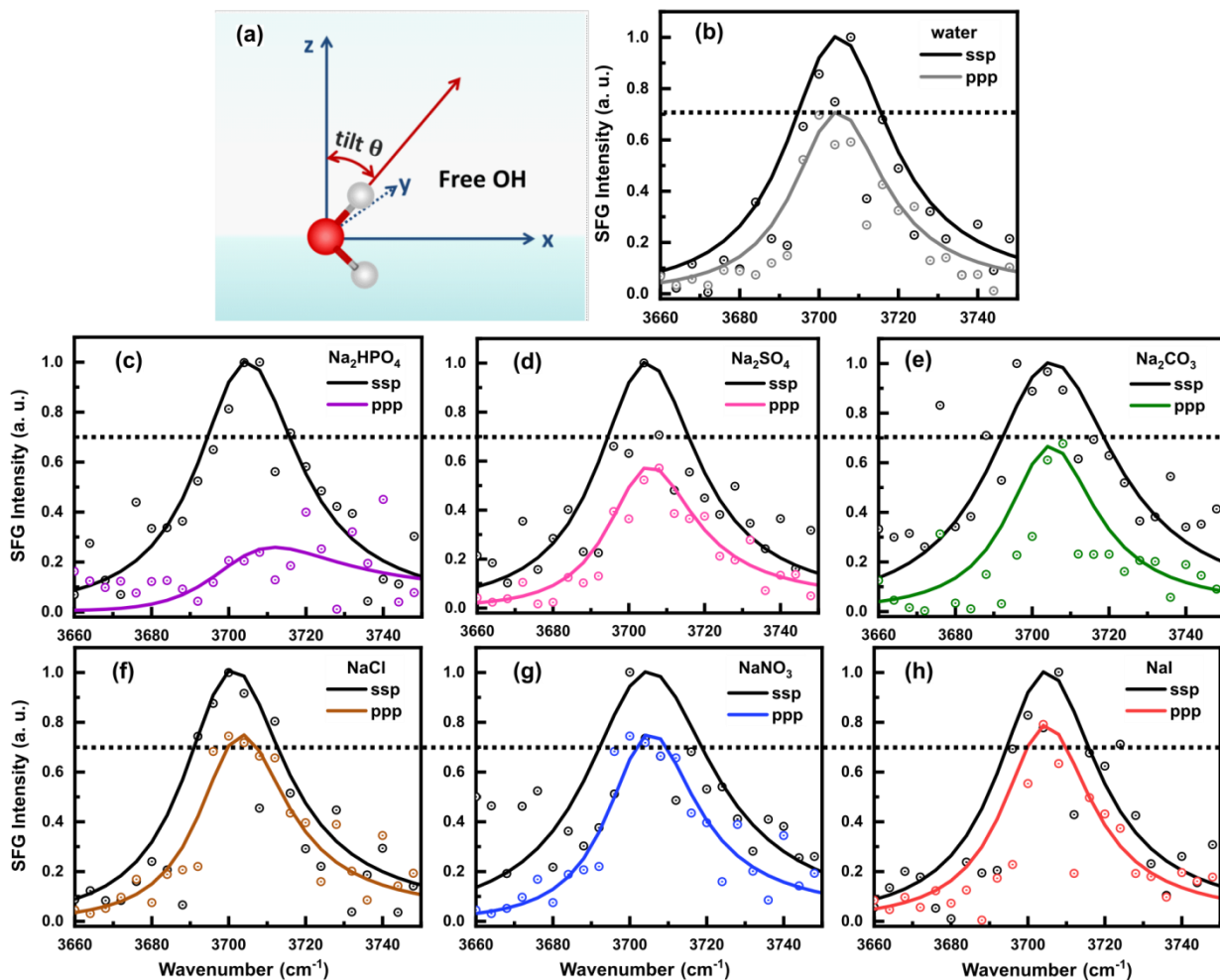


Figure 4. (a) Representation of orientation angle (tilt angle)  $\theta$  formed by free OH oscillator with the surface normal. (b)-(h) SFG intensity spectra for free OH oscillator at air/aqueous interface in the presence of various 1M Hofmeister series sodium salts in ssp and ppp-polarization schemes. The points show experimental data, and the solid lines are the Lorentzian fit curves. Fitting parameters are given in table S3 of the supporting information. The horizontal dotted line reflects the apparent ion-specific variation in ppp-spectral intensity of free OH peak compared to pristine air/water interface (b).

a broad region from 3000 to 3650  $\text{cm}^{-1}$  assigned with three peak positions at around 3230, 3445, and 3550  $\text{cm}^{-1}$ . The lowest frequency ensemble is attributed to strongly H-bonded (tetrahedral coordinated) water molecules, and the higher frequency peaks correspond to weakly H-bonded water molecules, however, the exact assignment of these peaks continues to be ambiguous.<sup>23,28,33,38-42</sup> The sharp peak at 3704  $\text{cm}^{-1}$  corresponds to the stretching mode of the non-hydrogen bonded free OH oscillator (dangling bond) of water molecules protruding out of the interface. The SFG intensity plots shown in figure 3 (c and d) reflect the water spectra in the presence of ions at the air/aqueous interface.<sup>28-29</sup> For our analysis, we considered the amplitude ratio of the peaks at 3445  $\text{cm}^{-1}$  and 3230  $\text{cm}^{-1}$  to estimate the strength of the H-bonding environment of water molecules present at the interface.<sup>39, 41</sup> It is quite evident from the SFG plots that the presence of ions significantly per-

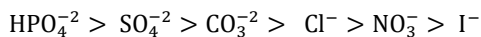
turbs the H-bonding environment of the water molecules. The relative enhancement in SFG intensity around 3230  $\text{cm}^{-1}$  in the presence of kosmotropes ( $\text{HPO}_4^{2-}$ ,  $\text{SO}_4^{2-}$ ,  $\text{CO}_3^{2-}$ ) and at 3445  $\text{cm}^{-1}$  for chaotropes ( $\text{NO}_3^-$  and  $\text{I}^-$ ) has been attributed to the size, charge, polarizability, and surface propensity of respective ions at the air/aqueous interface.<sup>28-29</sup> We have plotted the variation in relative oscillator strength as a function of ions present at the interface (figure 3e). The relative oscillator strength follows the Hofmeister series (equation 7), where the minimum value is observed for  $\text{HPO}_4^{2-}$ , and maximum in the presence of  $\text{I}^-$  indicating the ability of kosmotropes to make more strongly H-bonded water species at the interface compared to the neat air/water interface. In contrast, we witnessed an increase in the weakly H-bonded molecules in the presence of chaotropes. This ability of kosmotropes and chaotropes to alter the strength of H-bonded water molecules can be under-

stood as follows. It is known that due to their small size and low polarizability, kosmotrope anions are repelled from the interface and are strongly hydrolyzed.<sup>43</sup> Owing to the high charge density of kosmotropes, water molecules in their surrounding are closely packed and thus are strongly H-bonded.<sup>44-45</sup> In contrast, owing to the large size and high polarizability, chaotropes are adsorbed at the interface and are partially hydrolyzed by shedding their hydration sheath that results in weakly H-bonded water molecules.<sup>44,46</sup>

Figure 3f demonstrates the variation in the area under the free OH peak, integrated between 3660  $\text{cm}^{-1}$  and 3750  $\text{cm}^{-1}$ , as a function of various ions. An increasing trend is observed moving from kosmotropes to chaotropes, with minimum for  $\text{Na}_2\text{HPO}_4$  and a maximum value for NaI. This observation can naively be attributed to the enhanced population of free OH water molecules in the presence of chaotropes compared to kosmotropes at the interfacial region. However, a fuller understanding shows that the SFG signal intensity is proportional to  $N_S \langle \cos\theta \rangle$ . Here,  $N_S$  represents the number of molecules participating in the SFG process at the interface while  $\theta$  is the orientation angle.<sup>20, 33</sup> Therefore, the contribution from  $\theta$  cannot be ignored; for which, we must consider the contribution of the orientation of free OH oscillators towards the observed variation in the SFG intensity or integrated area.

We performed a quantitative analysis to determine the impact of Hofmeister ions on the orientation of free OH groups at the air/aqueous interface. Du *et al.*<sup>20</sup> first studied the orientation of free OH groups at the air/aqueous interface and this was subsequently investigated by various groups.<sup>47-50</sup> Figure 4 shows the recorded SFG spectra in ssp and ppp-polarization schemes at the air/aqueous interface in the presence of 1M sodium salts from 3660  $\text{cm}^{-1}$  to 3750  $\text{cm}^{-1}$ . For our analysis, we have normalized the ssp-SFG spectra and accordingly scaled the ppp-SFG spectra; which demonstrate the ion-specific perturbations in the free OH peak intensity. The free OH spectral profiles recorded in ssp and ppp-schemes are then utilized for the calculation of orientation angle of free OH oscillator with respect to the surface normal (figure 5a). The detailed theory and calculation of the orientation angle of free OH are discussed in sections S1 and S2-III of the supporting information.

For the pristine air/water interface, we determine the free OH angle to be 37.6° which is in close agreement with the values reported in the literature.<sup>20,48,50-51</sup> In comparison to the pristine air/water interface, we have observed an increase in free OH tilt angle in the presence of kosmotropes, whereas a small decrease is observed for chaotropes. Figure 5a (left axis) shows the variation in orientation angle of free OH as a function of ions present at the air/aqueous interface, which follows the Hofmeister series (equation1):



The free OH orientation angle is maximum  $\sim 48.4^\circ$  in the presence of  $\text{Na}_2\text{HPO}_4$ , and decreases as we move from kosmotropes to chaotropes (left to right, figure 5a) with a minimum value of 36.2° in the presence of NaI. This difference leads to a lower integrated free OH area for  $\text{Na}_2\text{HPO}_4$  compared to NaI. However the angle alone is not sufficient and there must

be almost a factor of 2 decrease in  $N_S$  for the kosmotrope. In the past, ion-specific orientation studies of free OH groups have not been explored in detail. A recent report by Feng *et al.* showed that the presence of NaF (kosmotrope) rotates the free OH group away from the surface normal.<sup>51</sup> This finding is in good agreement with our experimental observations of reorientation of free OH oscillator towards the air/aqueous interface in the presence of kosmotropic ions. The significant increase in free OH tilt angle in the presence of  $\text{HPO}_4^{-2}$  and  $\text{SO}_4^{-2}$  correlates well with the previously observed decrease in free OH peak area (figure 3f). However, for the case of chaotropes, the relative change in the orientation of the free OH group is quite small and is tilted more towards the surface normal. This indicates that the increase in the SFG signal for chaotropes (figure 3f) might have arisen due to an increase in the population of free OH groups at the interfacial region.

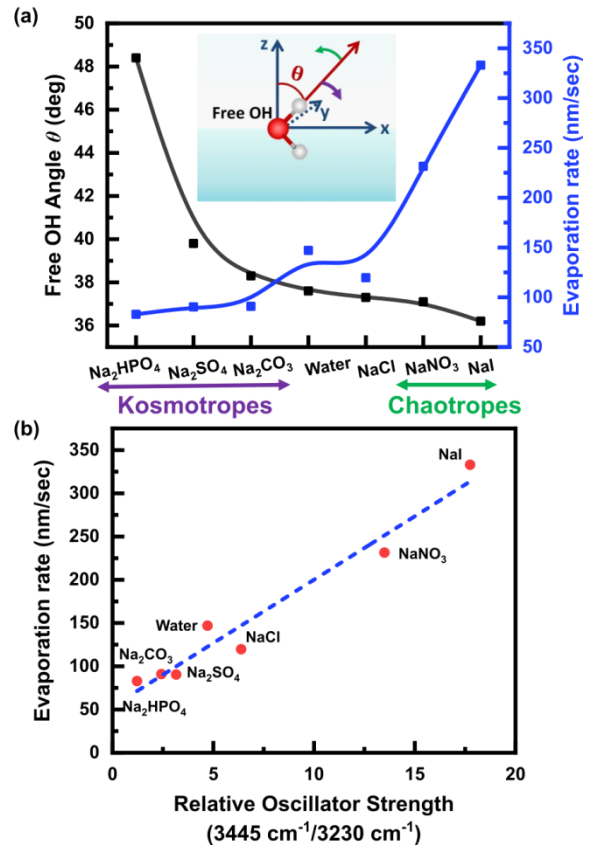


Figure 5. (a) Ion-specific variation in tilt angle values of free OH oscillator (left axis) in inverse correlation with the evaporation rates (right axis) studied at the air/aqueous interface. (b) Evaporation rates of the sessile droplets obtained from interferometry experiment (figure 2b) plotted as a function of relative OH oscillator strength observed from SFG spectra (figure 3c-d).

3f). However, for the case of chaotropes, the relative change in the orientation of the free OH group is quite small and is tilted more towards the surface normal. This indicates that the increase in the SFG signal for chaotropes (figure 3f) might have arisen due to an increase in the population of free OH groups at the interfacial region.

The right axis of figure 5a represents the ion-specific evaporation rates at the air/aqueous interface, which are found to follow an inverse correlation with the observed trend of free OH tilt angle in the presence of ions. Moreover, figure 5b provides a linear and direct correlation between the sessile droplet's evaporation rates (figure 2b) against the relative oscillator strength acquired from SFG spectra (figure 3e). Combining the observations from figure 5, we can conclude that the presence of kosmotropes ( $\text{HPO}_4^{-2}$ ,  $\text{SO}_4^{-2}$ , and  $\text{CO}_3^{-2}$ ) brings more strongly H-bonded water moieties to the air/aqueous interface, with free OH oscillators significantly tilted away from the surface normal and bonded OH embedded deeper into the bulk fluid. This, in turn, lowers the evaporation rates compared to the pristine air/water interface. However, with chaotropes ( $\text{NO}_3^-$  and  $\text{I}^-$ ), we find a more weakly H-bonded environment with a little reorientation of free OH oscillators towards the surface normal, resulting in a higher evaporation rate.

The impact of the strength of the H-bonding environment and orientation of the free OH oscillator on the evaporation process can be understood as follows: A water molecule possesses 9-degrees of freedom; 3-translational, 3-rotational, and 3-vibrational.<sup>16-17,19</sup> When a water molecule binds to other molecules, it loses degrees of freedom resulting in a reduction in its average energy,  $\langle E \rangle$ . In addition, the orientation of water OH oscillator plays an essential role in the formation of H-bonds<sup>50-52</sup> and hence, in turn, determines the average energy of surface water molecules. This is quite consistent with the reported molecular dynamics study, where Musolino *et al.* reported that the water molecule with dipole vector oriented more towards the surface normal loses its H-bonds with nearest neighbors and carries high average energies at the air/water interface.<sup>19</sup> In addition, the average energy difference between tetrahedral and monomer configuration of interfacial water molecule is found to be comparable with the enthalpy of vaporization that is 11.5kcal/mol.<sup>19</sup> To raise the clarity, we have plotted the variation in average energy of water molecule with number of H-bonds it donates and/or accepts with its neighbors (figure S4 in supporting information, the data has been adopted from Musolino *et al.*<sup>19</sup>). It is evident from the plot that the evaporating water molecule possess minimum average energy,  $\langle E \rangle$  for the tetrahedral configuration, and an increment in energy is observed when it breaks H-bonds with its surroundings at the interface. This indicates that the strongly H-bonded species and the conformation of surface water molecules with free OH groups tilted away from the surface normal as observed in the presence of kosmotropes belong to the configuration of low average energy. This lower energy configuration must be responsible for slowing down the evaporation process. In distinction, the possible decrease in the H-bonding strength of surface water molecules with the presence of enhanced population of free OH oscillators possess high average energies, accelerate the evaporation process for chaotropes. The present results state that the strongly/weakly H-bonded environment of water molecules as observed in the presence of kosmotropes/chaotropes defines the energy of the interfacial water molecules and consequently impacts the evaporation process. In summary, we show that the observed dependence of evaporation rate on added salts following the Hofmeister series, cannot be explained by surface tension arguments alone. We present clear evidence that the evaporation rate increases with (i) free OH group aligned more vertically resulting in (ii)

weaker H-bonding to neighbouring molecules (ratio of 3445/323) and (iii) increased number of water molecules present at the surface ( $N_s$ ).

## CONCLUSIONS

In summary, we have used surface-specific SFG vibrational spectroscopy and time-resolved interferometry to establish an intriguing correlation between the interfacial water structure (H-bonding and orientation of free OH oscillators) and the evaporation process. Structure making and breaking Hofmeister ions provided a platform to visualize the conformation of water molecules characteristic of slow/fast evaporation at the air/aqueous interface. Presence of kosmotropes ( $\text{HPO}_4^{-2}$ ,  $\text{SO}_4^{-2}$ , and  $\text{CO}_3^{-2}$ ) foster strongly H-bonded water molecules with an increase in the tilt angle of the free OH oscillators at the interface, slows down the evaporation. However, for the case of chaotropes ( $\text{NO}_3^-$  and  $\text{I}^-$ ), we find a more weakly H-bonded environment with little impact on the orientation of free OH oscillators, with possible enhanced population of free OH oscillators results in higher evaporation rate. These findings reveal a deeper fundamental insight into the prevailing concerns on evaporation. The outcomes of this work would help in designing interfacial water structures to manipulate the evaporation processes for future needs.

## ASSOCIATED CONTENT

**Supporting Information** includes a detailed quantitative description for the calculation of orientation angle of free OH oscillator at the air/aqueous interface; Plots on variation in droplet central thickness vs. time showing impact of concentration of ions on evaporation of sessile aqueous droplets, surface tension studies on 1M sodium salt solutions, Calculation of orientation angle of free OH oscillator, Average energy vs. Number of H-bonds; tables of Lorentzian fitting parameters of SFG spectra in ssp and ppp-polarization schemes, table of orientation angle values of the free OH at the air/aqueous interface in the presence of ions. This material is available free of charge via the Internet at <http://pubs.acs.org>.

## AUTHOR INFORMATION

### Corresponding Author

\* Kailash C. Jena- Department of Physics and Department of Biomedical Engineering, Indian Institute of Technology Ropar, Rupnagar, Punjab-140001, India

Email: [kcjena@iitrpr.ac.in](mailto:kcjena@iitrpr.ac.in)

### Authors

Bhawna Rana- Department of Physics, Indian Institute of Technology Ropar, Rupnagar, Punjab-140001, India

David J. Fairhurst - Department of Physics and Mathematics, School of Science and Technology, Nottingham Trent University, Nottingham, Clifton Campus, NG11 8NS, United Kingdom

### Author Contributions

All authors have given approval to the final version of the manuscript.

### Notes

The authors declare no competing financial interest.

## ACKNOWLEDGMENT

We are grateful to Jahur A. Mondal, Kamal P. Singh and Manoranjan Mishra for the fruitful discussions. K. C. J. sincerely acknowledges the financial support from the Indian Institute of Technology Ropar for the development of research infrastructure under central facility, SEED grants and the Science and Engineering Research Board (SERB), India (CRG/2018/004975). B. R. acknowledges the British Council for Newton Bhabha fund ID: 544025790 to provide an opportunity to collaborate and carry out research at Nottingham Trent University, United Kingdom.

## ABBREVIATIONS

VIS, Visible; IR, infrared; HWHM, Half width at half maxima; SFG, Sum frequency generation.

## REFERENCES

- (1) Li, Y.; Diddens, C.; Segers, T.; Wijshoff, H.; Versluis, M.; Lohse, D. Evaporating droplets on oil-wetted surfaces: Suppression of the coffee-stain effect. *Proc. Natl. Acad. Sci.* **2020**, *117* (29), 16756-16763.
- (2) Jing, J.; Reed, J.; Huang, J.; Hu, X.; Clarke, V.; Edington, J.; Housman, D.; Anantharaman, T. S.; Huff, E. J.; Porter, B.; Shenker, A.; Wolfson, E.; Hiort, C.; Kantor, R.; Aston, C.; Schwartz, D. C. Automated high resolution optical mapping using arrayed, fluid-fixed DNA molecules. *Proc. Natl. Acad. Sci.* **1998**, *95*(14), 8046-8051.
- (3) Squyres, S. W.; Grotzinger, J. P.; Arvidson, R. E.; Bell III, J. F.; Calvin, W.; Christensen, P. R.; Clark, B. C.; Crisp, J. A.; Farrand, W. H.; Herkenhoff, K. E.; Johnson, J. R.; Klingelhöfer, G.; Knoll, A. H.; McLennan, S. M.; McSween Jr., H. Y.; Morris, R. V.; Rice Jr., J. W.; Rieder, R.; Soderblom, L. A. In situ evidence for an ancient aqueous environment at Meridiani Planum, Mars. *Science* **2004**, *306* (5702), 1709-1714.
- (4) Wang, X.; Zhang, M.; Schubert, D. W.; Liu, X. Oil-Water Separation Polypropylene Foam with Advanced Solvent-Evaporation Induced Coexistence of Microspheres and Microporous Structure. *Macromol. Rapid Commun.* **2022**, *2200177*.
- (5) Tao, P.; Ni, G.; Song, C.; Shang, W.; Wu, J.; Zhu, J.; Chen, G.; Deng, T. Solar-driven interfacial evaporation. *Nat. Energy* **2018**, *3*(12), 1031-1041.
- (6) Brutin, D.; Sobac, B.; Loquet, B.; Sampol, J. Pattern formation in drying drops of blood. *J. of fluid Mech.* **2011**, *667*, 85-95.
- (7) Rosenfeld, D.; Lohmann, U.; Raga, G. B.; O'Dowd, C. D.; Kulmala, M.; Fuzzi, S.; Reissell, A.; Andreae, M. O. Flood or drought: how do aerosols affect precipitation?. *Science*, **2008**, *321*(5894), 1309-1313.
- (8) Rosenfeld, D. Suppression of rain and snow by urban and industrial air pollution. *Science* **2000**, *287*(5459), 1793-1796.
- (9) Clement, A. C.; Burgman, R.; Norris, J. R. Observational and model evidence for positive low-level cloud feedback. *Science* **2009**, *325*(5939), 460-464.
- (10) Moore, F. G.; Richmond, G. L. Integration or segregation: how do molecules behave at oil/water interfaces?. *Acc. Chem. Res.* **2008**, *41*(6), 739-748.
- (11) Ji, N.; Ostroverkhov, V.; Tian, C. S.; Shen, Y. R. Characterization of vibrational resonances of water-vapor interfaces by phase-sensitive sum-frequency spectroscopy. *Phys. Rev. Lett.* **2008**, *100*(9), 096102.
- (12) Pahlavan, A. A.; Yang, L.; Bain, C. D.; Stone, H. A. Evaporation of Binary-Mixture Liquid Droplets: The Formation of Picoliter Pancakelike Shapes. *Phys. Rev. Lett.* **2021**, *127*(2), 024501.
- (13) Li, Y.; Diddens, C.; Lv, P.; Wijshoff, H.; Versluis, M.; Lohse, D. Gravitational effect in evaporating binary microdroplets. *Phys. Rev. Lett.* **2019**, *122*(11), 114501.
- (14) Jaiswal, V.; Dwivedi, R. K.; Hari Krishnan, A. R.; Dhar, P. Magnetohydrodynamics-and magnetosolutal-transport-mediated evaporation dynamics in paramagnetic pendant droplets under field stimulus. *Phys. Rev. E* **2018**, *98*(1), 013109.
- (15) Edwards, A. M. J.; Atkinson, P. S.; Cheung, C. S.; Liang, H.; Fairhurst, D. J.; Ouali, F. F. Density-driven flows in evaporating binary liquid droplets. *Phys. Rev. Lett.* **2018**, *121*(18), 184501.
- (16) Varilly, P.; Chandler, D. Water evaporation: A transition path sampling study. *J. Phys. Chem. B* **2013**, *117*(5), 1419-1428.
- (17) Mason, P. E. Molecular dynamics study on the microscopic details of the evaporation of water. *J. Phys. Chem. A* **2011**, *115*(23), 6054-6058.
- (18) Nagata, Y.; Usui, K.; Bonn, M. Molecular mechanism of water evaporation. *Phys. Rev. Lett.* **2015**, *115*(23), 236102.
- (19) Musolino, N.; Trout, B. L. Insight into the molecular mechanism of water evaporation via the finite temperature string method. *J. Chem. Phys.* **2013**, *138*(13), 134707.
- (20) Du, Q.; Superfine, R.; Freysz, E.; Shen, Y. R. Vibrational spectroscopy of water at the vapor/water interface. *Phys. Rev. Lett.* **1993**, *70*(15), 2313.
- (21) Mondal, J. A.; Nihonyanagi, S.; Yamaguchi, S.; Tahara, T. Three distinct water structures at a zwitterionic lipid/water interface revealed by heterodyne-detected vibrational sum frequency generation. *J. Am. Chem. Soc.* **2012**, *134*(18), 7842-7850.
- (22) Scheu, R.; Rankin, B. M.; Chen, Y.; Jena, K. C.; Ben-Amotz, D.; Roke, S. Charge asymmetry at aqueous hydrophobic interfaces and hydration shells. *Angew. Chem.* **2014**, *126*(36), 9714-9717.
- (23) Chaudhary, S.; Kaur, H.; Kaur, H.; Rana, B.; Tomar, D.; Jena, K. C. Probing the Bovine Hemoglobin Adsorption Process and its Influence on Interfacial Water Structure at the Air-Water Interface. *Appl. Spectrosc.* **2021**, *75*(12), 1497-1509.
- (24) Tyrode, E.; Johnson, C. M.; Kumpulainen, A.; Rutland, M. W.; Claesson, P. M. Hydration state of nonionic surfactant monolayers at the liquid/vapor interface: Structure determination by vibrational sum frequency spectroscopy. *J. Am. Chem. Soc.* **2005**, *127*(48), 16848-16859.
- (25) Hofmeister, F. Zur Lehre Von Der Wirkung Der Salze. *Naunyn-Schmiedeberg's Arch. Pharmacol.* **1888**, *25*, 1-30
- (26) Chen, X.; Yang, T.; Kataoka, S.; Cremer, P. S. Specific ion effects on interfacial water structure near macromolecules. *J. Am. Chem. Soc.* **2007**, *129*(40), 12272-12279.
- (27) Roy, S.; Mondal, J. A. Kosmotropic Electrolyte (Na<sub>2</sub>CO<sub>3</sub>, NaF) Perturbs the Air/Water Interface through Anion Hydration Shell without Forming a Well-Defined Electric Double Layer. *J. Phys. Chem. B* **2021**, *125*(16), 3977-3985.
- (28) Jubb, A. M.; Hua, W.; Allen, H. C. Organization of water and atmospherically relevant ions and solutes: vibrational sum frequency spectroscopy at the vapor/liquid and liquid/solid interfaces. *Acc. Chem. Res.* **2012**, *45*(1), 110-119.
- (29) Tian, C.; Byrnes, S. J.; Han, H. L.; Shen, Y. R. Surface propensities of atmospherically relevant ions in salt solu-

- tions revealed by phase-sensitive sum frequency vibrational spectroscopy. *J. Phys. Chem. Lett.* **2011**, 2(15), 1946-1949.
- (30) Piatkowski, L.; Zhang, Z.; Backus, E. H.; Bakker, H. J.; Bonn, M. Extreme surface propensity of halide ions in water. *Nat. Commun.* **2014**, 5(1), 1-7.
- (31) O'Brien, J. T.; Prell, J. S.; Bush, M. F.; Williams, E. R. Sulfate ion patterns water at long distance. *J. Am. Chem. Soc.* **2010**, 132(24), 8248-8249.
- (32) Verma, G.; Singh, K. P. Time-resolved interference unveils nanoscale surface dynamics in evaporating sessile droplet. *Appl. Phys. Lett.* **2014**, 104(24), 244106.
- (33) Tomar, D.; Rana, B.; Jena, K. C. The structure of water–DMF binary mixtures probed by linear and nonlinear vibrational spectroscopy. *J. Chem. Phys.* **2020**, 152(11), 114707.
- (34) Kaur, H.; Chaudhary, S.; Kaur, H.; Chaudhary, M.; Jena, K. C. Hydrolysis and Condensation of Tetraethyl Orthosilicate at the Air–Aqueous Interface: Implications for Silica Nanoparticle Formation. *ACS Appl. Nano Mater.* **2021**, 5(1), 411-422.
- (35) Jena, K. C.; Covert, P. A.; Hore, D. K. The effect of salt on the water structure at a charged solid surface: Differentiating second- and third-order nonlinear contributions. *J. Phys. Chem. Lett.* **2011**, 2(9), 1056-1061.
- (36) Azam, M. S.; Cai, C.; Gibbs, J. M.; Tyrode, E.; Hore, D. K. Silica surface charge enhancement at elevated temperatures revealed by interfacial water signals. *J. Am. Chem. Soc.* **2020**, 142(2), 669-673.
- (37) Troiano, J. M.; McGeachy, A. C.; Olenick, L. L.; Fang, D.; Liang, D.; Hong, J.; Kuech T. R.; Caudill E. R.; Pedersen J. A.; Cui Q.; Geiger, F. M. Quantifying the electrostatics of polycation–lipid bilayer interactions. *J. Am. Chem. Soc.* **2017**, 139(16), 5808-5816.
- (38) Rogers, M. M.; Neal, J. F.; Saha, A.; Algarni, A. S.; Hill, T. C.; Allen, H. C. The Ocean's Elevator: Evolution of the Air–Seawater Interface during a Small-Scale Algal Bloom. *ACS Earth Space Chem.* **2020**, 4(12), 2347-2357.
- (39) Strazdaite, S.; Versluis, J.; Backus, E. H.; Bakker, H. J. Enhanced ordering of water at hydrophobic surfaces. *J. Chem. Phys.* **2014**, 140(5), 054711.
- (40) Dalchand, N.; Dogangun, M.; Ohno, P. E.; Ma, E.; Martinson, A. B.; Geiger, F. M. Perturbation of hydrogen-bonding networks over supported lipid bilayers by poly (allylamine hydrochloride). *J. Phys. Chem. B* **2019**, 123(19), 4251-4257.
- (41) Smolentsev, N.; Smit, W. J.; Bakker, H. J.; Roke, S. The interfacial structure of water droplets in a hydrophobic liquid. *Nat. Commun.* **2017**, 8(1), 1-6.
- (42) Ishiyama, T.; Morita, A. Nuclear quantum effect on the  $\chi$  (2) band shape of vibrational sum frequency generation spectra of normal and deuterated water surfaces. *J. Phys. Chem. Lett.* **2019**, 10(17), 5070-5075.
- (43) Levin, Y.; Dos Santos, A. P.; Diehl, A. Ions at the air-water interface: an end to a hundred-year-old mystery?. *Phys. Rev. Lett.* **2009**, 103(25), 257802.
- (44) Parsons, D. F.; Boström, M.; Nostro, P. L.; Ninham, B. W. Hofmeister effects: interplay of hydration, nonelectrostatic potentials, and ion size. *Phys. Chem. Chem. Phys.* **2011**, 13(27), 12352-12367.
- (45) Herman, K. M.; Heindel, J. P.; Xantheas, S. S. The many-body expansion for aqueous systems revisited: III. Hofmeister ion–water interactions. *Phys. Chem. Chem. Phys.* **2021**, 23(19), 11196-11210.
- (46) Heindel, J. P.; Xantheas, S. S. The many-body expansion for aqueous systems revisited: II. Alkali metal and halide ion–water interactions. *J. Chem. Theory Comput.* **2021**, 17(4), 2200-2216.
- (47) Wei, X.; Shen, Y. R. Motional effect in surface sum-frequency vibrational spectroscopy. *Phys. Rev. Lett.* **2001**, 86(21), 4799.
- (48) Gan, W.; Wu, D.; Zhang, Z.; Feng, R. R.; Wang, H. F. Polarization and experimental configuration analyses of sum frequency generation vibrational spectra, structure, and orientational motion of the air/water interface. *J. Chem. Phys.* **2006**, 124(11), 114705.
- (49) Sun, S.; Tang, F.; Imoto, S.; Moberg, D. R.; Ohto, T.; Paesani, F.; Bonn, M.; Backus, E. H. G.; Nagata, Y. Orientational distribution of free OH groups of interfacial water is exponential. *Phys. Rev. Lett.* **2018**, 121(24), 246101.
- (50) Boily, J. F.; Fu, L.; Tuladhar, A.; Lu, Z.; Legg, B. A.; Wang, Z. M.; Wang, H. Hydrogen bonding and molecular orientations across thin water films on sapphire. *J. Colloid Interface Sci.* **2019**, 555, 810-817.
- (51) Feng, R. R.; Guo, Y.; Wang, H. F. Reorientation of the “free OH” group in the top-most layer of air/water interface of sodium fluoride aqueous solution probed with sum-frequency generation vibrational spectroscopy. *J. Chem. Phys.* **2014**, 141(18), 18C507.
- (52) Luzar, A.; Chandler, D. Hydrogen-bond kinetics in liquid water. *Nature* **1996**, 379(6560), 55-57.

